WFOS CoDP1 Down-Select

Summary and Team Recommendation

Version 2.2

2018-Mar-20

Contents

1 Executive Summary

In May 2017, the WFOS Opto-Mechanical Design Requirements phase concluded with the consensus that a cross-dispersing design approach to achieving medium spectral resolution ($R \sim 5000$) at a useful multiplex was too risky to pursue. In response, the WFOS team embarked on an urgent trade study of alternate WFOS designs. This report summarizes the work accomplished during this phase and presents a recommendation on how to carry these designs forward.

The three designs under consideration are known as Slicer-WFOS, XChange-WFOS, and Fiber-WFOS. The first two are variants on a rotating, 2-channel monolithic spectrograph that each achieve the spectral resolution goals of WFOS in different ways. From the perspective of an observer, the capabilities of these designs are not dissimilar from the baseline concept studied in the OMDR phase as well as previous versions of MOBIE. Over an $8.3' \times 3'$ field, they provide low-resolution ($R \sim 1500$) spectroscopy for a maximum of ∼100 targets. To reach $R \sim 5000$, Slicer-WFOS would insert slit-slicing modules in the focal plane that slice a nominal $0.75''$-wide slit into three narrower "slitlets" and re-image these side-by-side, thus reducing the maximum multiplex by a factor of three. XChange-WFOS, on the hand, achieves medium resolution by exchanging multiple VPH gratings and articulating the cameras in each channel to match a desired wavelength range. While the multiplex is fixed, XChange-WFOS requires 3–6 exposures to cover the full wavelength range at $R \sim 5000$.

Fiber-WFOS is a modular fiber-based design that deploys fiber bundles mounted on robotic positioners across the focal plane to achieve a high multiplex advantage while providing full wavelength coverage (310–1000 nm) at $R \sim 5000$ for every target. The fiber output is fed to an array of fixed, mounted spectrographs, each with 4 wavelength channels. The full instrument would populate 9 spectrographs and deploy 700 bundles across a $10'$ field-of-view, but to address budget constraints, we present a stage-1 concept (Fiber-WFOS Stage-1) with 6 spectrographs (468 bundles) that could be expanded to its full potential at a later stage.

Comparing Slicer-WFOS and XChange-WFOS, we find the challenge of slicer module placement, positional and angular precision, and manufacturing tolerance to be unfortunate limitations. Instead, it is our belief that XChange-WFOS is the best monolithic concept put forward for WFOS so far. It offers flexibility at both the focal plane (standard slitmask design) and for spectral modes, which can be set independently in each channel. It also offers various options for achieving even higher spectral resolution and is the only design of the three to provide an imaging mode. Fiber-WFOS, however, provides roughly order-of-magnitude advantages in terms of its overall ability to gather information (i.e., survey speed), especially for samples of ∼100 objects or more, as desired by many of the WFOS core science programs. The resolved spatial information from fiber bundles is also valuable, enabling faster and more robust transient followup and opening new science territory especially when combined with GLAO.

The team feels that the advantages of Fiber-WFOS are compelling, but recognizes the perception that fiber-based instruments carry significant performance risks. Major problems with early-generation fiber instruments have now been understood and can be mitigated with improved designs and new technology. Still, to address whether the 0.1% background subtraction precision required by WFOS can be achieved with fibers, an extensive study of existing fiber instrument data has been conducted during this phase with reassuring results that show negligible contributions from fiber systematics in continuum precision and sky emission line subtraction.

Given this, our recommendation is that Fiber-WFOS be pursued in the next design phase with a focus on further risk reduction in preparation for a full Conceptual Design Review (CoDR) in Fall 2019. Meanwhile, we recommend maintaining XChange-WFOS as a viable back-up option should the outcome of CoDR find an increased risk assessment for Fiber-WFOS or reveal new problems. The Fall 2019 timing would also allow initial performance assessments from DESI and PFS, major fiber-based facilities that will emerge from commissioning next year.

2 Introduction

TMT's Wide Field Optical Spectrograph (WFOS) was adopted as an early-light instrument concept for in 2006. It is foremost a natural-seeing multi-object spectrograph operating at optical wavelengths with the ability to access a significant fraction of TMTs available ∼20 arcmin diameter field-of-view, hence WFOSs "wide field" designation. It is also intended for rapid followup of transient sources and was envisioned for extremely faint spectroscopy.

The large physical size of the TMT Nasmyth focal plane combined with the desire to reach spectral resolutions of $R \sim 5000$ with a useful degree of multiplex have posed significant challenges for WFOS instrument concepts. At the conclusion of the Opto-Mechanical Design Requirements (OMDR) phase in May 2017, it was clear that the cross-dispersing architecture central to the original MOBIE design led to risks in instrument packaging, spectral layout, stray light baffling options and optical component size. Meanwhile, the end-to-end throughout performance of the "OMDR Baseline" design struggled to meet requirements. The conclusion from the External OMDR Review was that the team should explore two alternative design paths for achieving WFOS's essential capabilities. This summary document reports on the analysis and team recommendations from this 8-month trade study.

The first path explores variations on the "monolithic" design familiar to previous WFOS iterations in which optical components share the same light path from the focal plane to detector. Our initial focus here was on "Slicer-WFOS" which employs image slicers at the focal plane to yield effectively narrower slits when $R \sim 5000$ is desired. A number of challenges arose in this design over the course of our study that motivated us to explore an alternative: XChange-WFOS. This concept uses a regular slitmask but enables different modes for spectral resolution and wavelength coverage through the exchange of a series of VPH gratings. Desired wavelength channels are turned by articulating cameras with respect the grating and beam angle. While we had less time to develop XChange-WFOS, we believe it is a more compelling option for a slit-based monolithic WFOS design than Slicer-WFOS.

The second design path is modular, employing bundles of optical fibers to divide the focal plane and direct light to an array of replicated spectrographs. The essential components share commonalities with other fiber instruments such as those deployed by SDSS, VLT GIRAFFE, VLT MOONS, DESI, and PFS. A straw-man fiber design was presented at the conclusion of OMDR and demonstrated promise. The work here represents a full feasibility study and initial costing. Concerns over fiber response stability and its impact on sky subtraction was a major topic of study in this phase.

2.1 Preparation of This Document

This document was prepared in March 2018 by Kevin Bundy (WFOS Principal Investigator) with help from Chuck Steidel (WFOS Project Scientist), Maureen Savage (WFOS Project Manager), Nick MacDonald (WFOS Senior Engineer), Renate Kupke (WFOS Lead Optical Designer), and Matthew Radovan (WFOS Lead Engineer). The analysis and designs presented here represents the hard work in a short amount of time by the very talented WFOS team.

2.2 Applicable Documents

We list documents produced for the current Conceptual Design Phase-I "Down-select" and trade studies.

Fiber-WFOS Documentation:

Fiber-WFOS: Focal Plane & Structure [TMT.INS.PRE.18.033.DRF01] — Focal plane system, robotic positioners, fiber run, mechanical structure.

Fiber-WFOS: Spectrograph Design [TMT.INS.PRE.18.035.DRF01] — Unit fiber spectrograph design concept.

Fiber-WFOS: MLA and Fore-Optics [TMT.INS.PRE.18.040.DRF01] — Micro-lens array and fiber bundle fore-optics.

Fiber Systematics and Sky Subtraction [TMT.INS.JOU.18.002.DRF01] — Draft manuscript containing analysis on the impact of fiber systematics on instrument stability and sky subtraction.

Fiber-WFOS: Target Allocation [TMT.INS.TEC.18.007.DRF01] — Simulations of targeting efficiency and completeness used to define robotic positioner specifications.

Fiber-WFOS: Guider Requirements [TMT.INS.PRE.18.027.DRF01] — Guide star availability analysis used to update guider camera requirements.

Fiber-WFOS: Alternate Blue Camera [TMT.AOS.TEC.18.021.DRF01] — Alternative blue camera design for the fiber spectrograph.

Fiber-WFOS: Spectrograph Literature Study [TMT.INS.PRE.18.026.DRF01] — A literature study of existing fiber-based spectrograph designs.

Detector Concepts [TMT.INS.PRE.18.032.DRF01] — Applicable detector technology.

Slicer-WFOS Documentation:

Slicer-WFOS: Slicer Module Design [TMT.INS.PRE.18.028.DRF01] — Design for the slit slicer modules.

Slicer-WFOS: Module Placement and Mask Structure [TMT.INS.PRE.18.028.DRF01] — Module positioning, focal plane, and mask system.

Nikon Camera Design [TMT.INS.TEC.18.011.DRF01] — Nikon camera designs.

Slicer-WFOS Documentation:

XChange-WFOS: Optical and Structural Layout [TMT.INS.PRE.18.044.DRF01] — Optical and structural layout for XChange-WFOS.

General Documents and Additional References:

Risk Assessment [TMT.INS.PRE.18.037.DRF01] — Risk assessment for Fiber-WFOS and XChange-WFOS.

OMDR Science Definitions and Design Drivers [TMT.INS.TEC.17.007.REL01] — WFOS science capabilities, competitive landscape, and requirements updated in May 2017.

MOBIE OCDD [TMT.INS.DRD.08.004.DRF01] — The MOBIE instrument's Operational Concepts Definition Document (OCDD) from 2008.

3 Design Overview

In this section, we present a high-level description of the design concepts and refer to additional submitted documentation for further details. Key aspects of performance, risk, and cost are considered in the design comparisons discussed in Section 4.

3.1 Slicer-WFOS

The optical layout for Slicer-WFOS is a variant on the 2-channel low-resolution ($R \sim 1500$) mode for the OMDR Baseline design, with the important difference of a transmissive VPH grating architecture that allows gentler camera angles and therefore much easier mechanical packaging. With the prism removed and far more beam clearance, the camera's pupil relief can be reduced and the cameras made smaller. Note that the fixed and transmissive nature of dispersive architecture prevents an imaging mode for Slicer-WFOS.

The inspiration for an image slicer comes from Bernard Delabre (a long-time WFOS external reviewer) who recognized that the fact that detector pixels (0.05 arcsec) oversample the 0.75 arcsec slitwidth enables full use of spectra from much narrower slits and effectively higher spectral resolution. A 0.25 arcsec wide slit would deliver $R \sim 5000$ with appropriate sampling but would suffer aperture losses in typical seeing with FWHM of 0.5 arcsec. A slit slicer overcomes the aperture loss by slicing the slit along the long

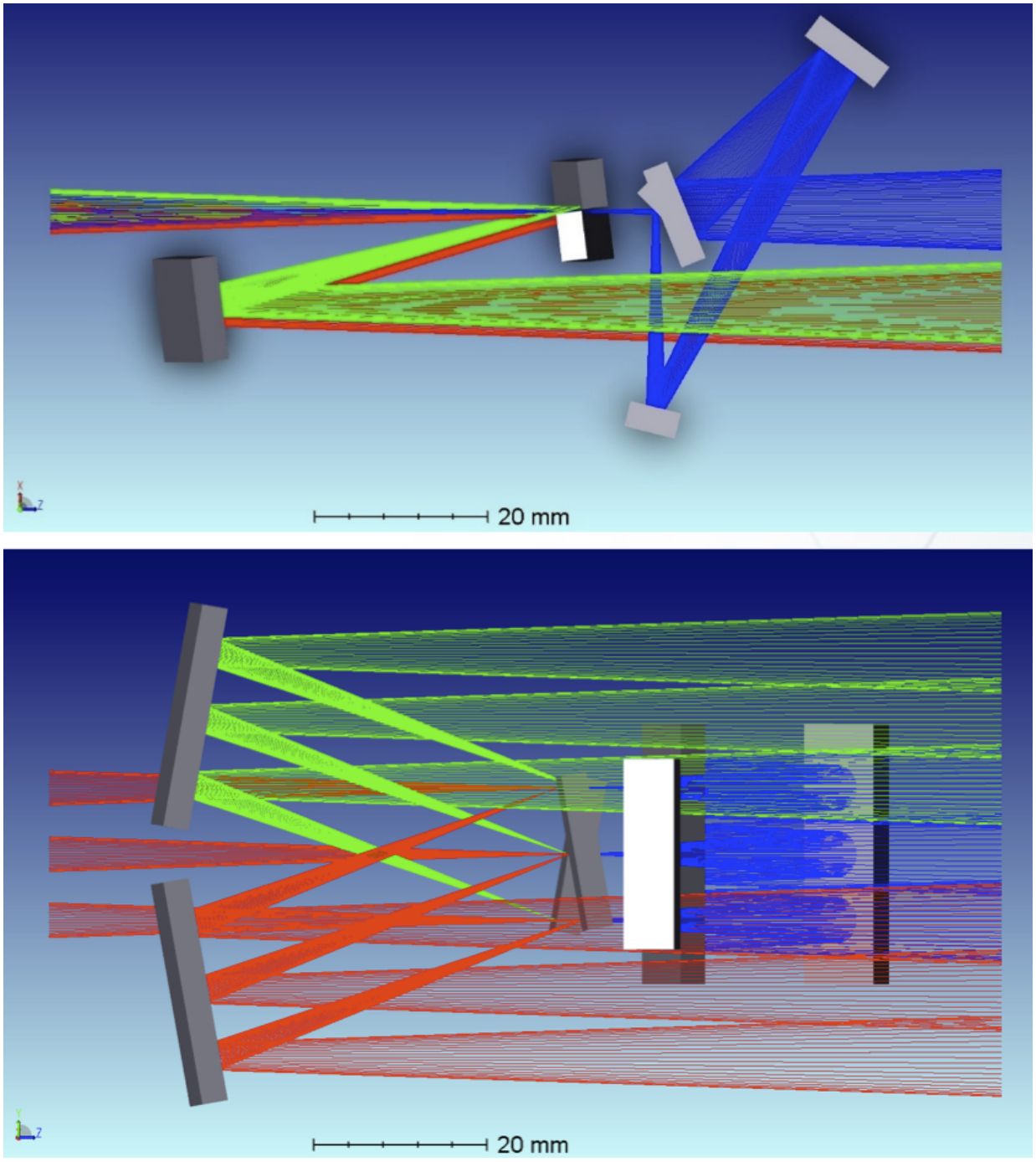

Figure 1: Optical layout seen from two vantage points of a single slicer module for Slicer-WFOS. Different ray colors correspond to incident light at the center (blue), upper third (green), and lower third (red) of the nominal 0.75″-wide slit. The use of flat mirrors reduces aberrations and sensitivity to tilt, but a mirror system for the central slitlet is also required to make all path lengths uniform (see Slicer-WFOS: Slicer Module Design).

(spatial) axis into three. Through a series of mirrors, the upper and lower slices can be re-imaged to either side of the central slit. Each of the three slitlets delivers $R \sim 5000$, but can be recombined to recover all the flux normally incident on a 0.75 arcsec wide slit.

Implementing this slit slicing leads to a Slicer-WFOS instrument with three key components. First is the spectrograph, composed of the collimator, dichroic, VPH gratings and cameras. These components must be held in a rotating structure (rotating as a given field tracks across the sky) with excellent flexure control. Second is the slicer module, with a series of mirrors that must be carefully aligned and assembled for use in specific parts of the focal plane (see Figure 1). A significant challenge is the strong curvature of the focal surface ($R = 3$ m) compared to the relatively fixed angle of the chief ray compared to optical axis as a function of field position. The third major component is the focal plane plugging system that would allow slicer modules to be placed in a mask and held with sufficient angular precision, while providing a way to change out the mask for a new one when the user wishes to observe a new set of objects.

In our final design for Slicer-WFOS, we envision 25 slicer modules whose layout and design is described in the Slicer-WFOS: Slicer Module Design report. The mechanical structure for the mask and two options for the module placement system is presented in Slicer-WFOS: Module Placement and Mask Structure. One option would require the set of ∼10 masks desired for a given night to be plugged manually during the day. The following day, the modules would be unplugged and inserted into the new set of masks. In the alternative system, a pick-and-place robot configures modules on the next observing while a current mask is being observed. Here, only two sets of modules would be required.

We believe our design work leads to the conclusion that Slicer-WFOS is not a compelling choice for a number of reasons. The fact that different slicer designs are required for different parts of the focal plane introduces an additional level of complexity with implications for plugging operations and instrument calibration. Meeting requirements on telecentricity precision was also difficult. The plugging operations themselves appear to be tedious, with significant effort required to ensure that a robotic solution was viable. Finally, experience with slicers in MUSE has demonstrated significant variation in instrument response (throughput, wavelength calibration, line-spread function) and the MUSE slicers remain stationary. The potential problems with instrument stability (and therefore sky subtraction) resulting from flexing of the modules at the focal plane could be daunting.

3.2 XChange-WFOS

Minimizing the "number of moving parts" was one of the driving philosophies in previous WFOS designs. But in relaxing this requirement we open new options for a monolithic WFOS design and address the challenges that arose with Slicer-WFOS.

XChange-WFOS trades the complexity of positioning slicers at the focal plane for additional complexity in the dispersing architecture. At low resolution ($R \sim 1500$), the XChange-WFOS and Slicer-WFOS concepts are nearly identical, but when XChange-WFOS is asked to achieve higher resolution, a series of VPH gratings can be exchanged in each channel with a robotic arm (Figure 3). A particular wavelength range and resolution combination demands a particular angular alignment between the incoming beam, a specified grating, and the camera (see XChange-WFOS: Optical and Structural Layout and Figure 2). Gratings and cameras are therefore mounted on articulating stages. Our current design borrows heavily from the Keck KCWI concept, although aside from the IFU capability, XChange-WFOS exhibits an important difference: the spectrograph, including the articulating components, must rotate as we track a field across the sky.

It should be noted that at medium resolution ($R \sim 5000$), 4–6 camera-grating-angle configurations are required to cover the full bandpass in each channel (Figure 4). We expect 6–8 minutes total would be required to rotate the instrument to the exchange position, exchange the grating, and re-acquire the field. The use of a standard slitmask maintains the maximum multiplex (∼100 slits) for all configurations. The primary benefit of Slicer-WFOS is flexibility. Each channel can be configured in its own spectral mode, and space for a series of gratings allows for an $R \sim 3500$ mode and future custom gratings. By inserting a

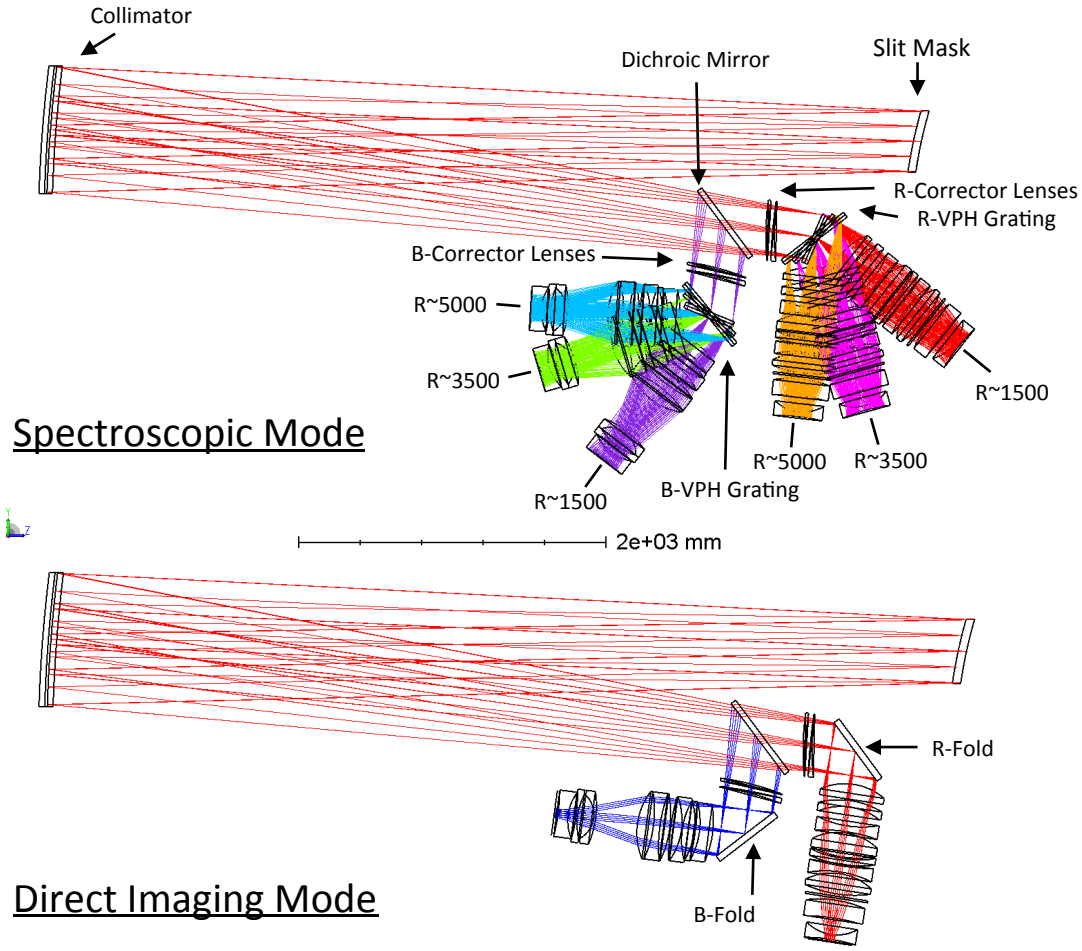

Figure 2: Optical layout for XChange-WFOS illustrating how different camera angles are required for different spectral resolution modes (top). Finer angular articulation with a specific grating defines the desired wavelength range. The optical layout in direct imaging mode is shown at bottom.

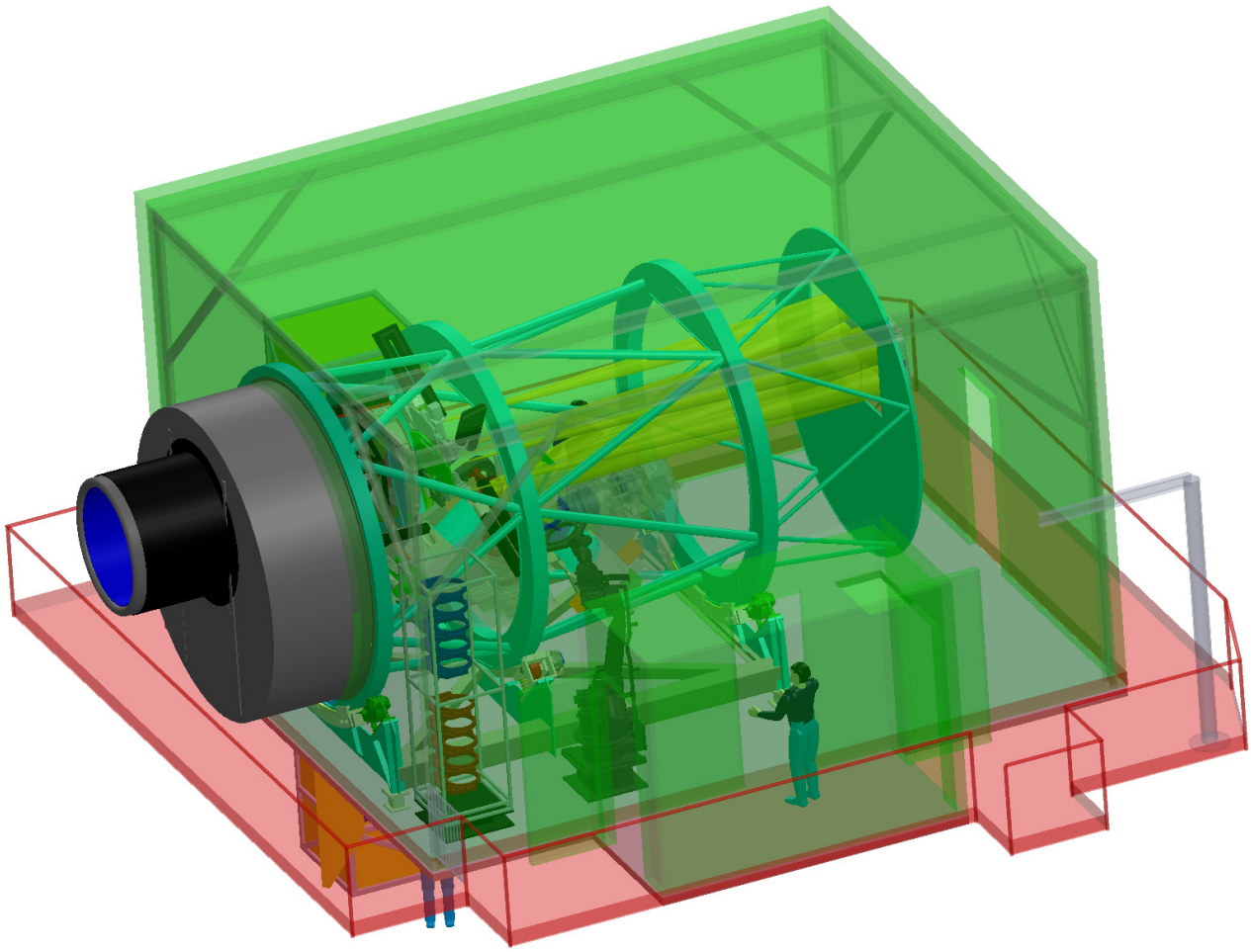

Figure 3: Structure design concept for XChange-WFOS. A robot transfers gratings stored beside the instrument into grating stages in both channels.

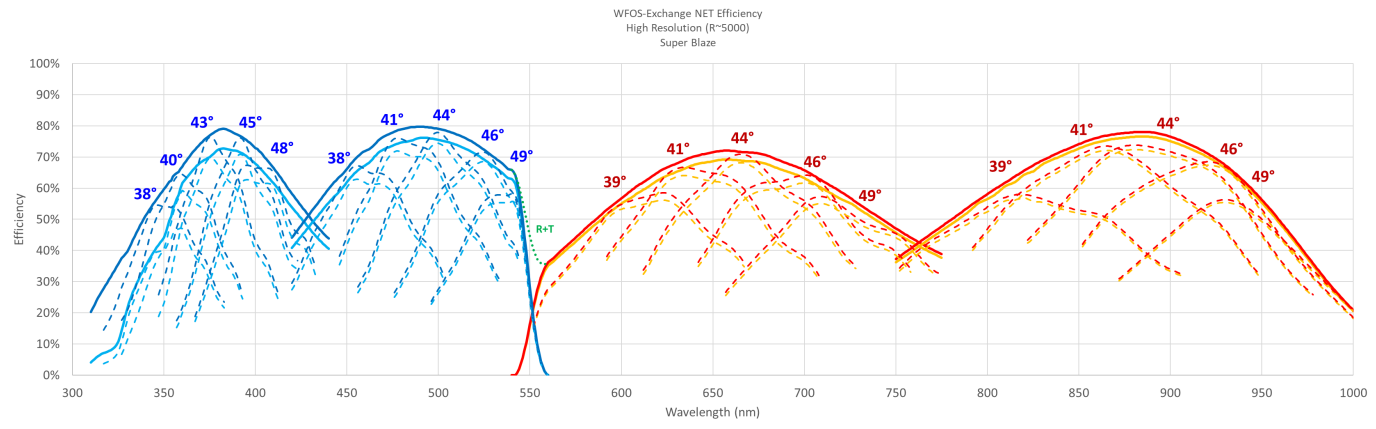

Figure 4: XChange-WFOS wavelength channels at $R \sim 5000$. Multiple exposures with different wavelength set-ups can be used to cover the desired wavelength range. Upper curves assume forthcoming technological advances in VPH gratings and make throughput assumptions that are more optimistic than those used to make Figure 8.

mirror, an imaging mode becomes available, making XChange-WFOS the only design studied in this phase that supports full-field imaging.

3.3 Fiber-WFOS

Fiber-WFOS addresses challenges in the monolithic designs by using optical fibers to decouple the focal plane from the spectrographs. The size of the fiber then determines the size of the spectrograph and influences the spectral resolution that can be easily achieved. Unlike other single-fiber instruments, Fiber-WFOS deploys "bundles" of 7 hexagonally-packed fibers that are coupled to nearly 100% fill-factor microlens arrays (see Fiber-WFOS: MLA and Fore-Optics). This approach maintains a modest fiber size (core diameter 155 μm) while subtending sufficient solid angle (0.75 arcsec^2) for seeing-limited and extended-source observations given TMT's large physical plate scale. Each 7-fiber bundle would subtend $\sim 1''$ on the sky and each fiber in the bundle would project to an on-sky diameter of $\sim 0.35''$.

The Fiber-WFOS instrument system is made of several key components (see Fiber-WFOS: Focal Plane & Structure and Figure 5). The rotating focal plane system houses 700 robotic positioners that allow the fiber bundles[1] to patrol a 22 arcsec radius, well matched to target densities in WFOS core science programs. In this phase, we have studied θ-ϕ positioners, which for Fiber-WFOS can be $\sim$3 times larger than similar components for DESI or PFS, although a z-stage is required to track the focal surface across the patrol zone. We are also interested in exploring alternative technologies like Starbugs. With its modular design, the focal plane positioning system can serve as a facility instrument for TMT, providing positioning for future fiber-based instruments (e.g., a high-resolution spectrograph) installed nearby.

From the back of the focal plane, a short run of fibers ($\sim$10 m) is maintained in a stress-relieving cable wrap and distributed to a series of fixed-mounted, replicated spectrographs (see Fiber-WFOS: Spectrograph Design). Each spectrograph accepts 546 fibers, delivering $R \sim 5000$ spectra spanning 310-1000 nm across 4 wavelength channels. With the current spectrograph design, 9 spectrographs are required for the maximum multiplex of 700 collecting bundles, a number that is set by the maximum possible diameter of the atmospheric dispersion corrector[2] (ADC). Given initial cost estimates, we recommend building the first 6 spectrographs (Fiber-WFOS Stage-1) and phasing in deployment of the remaining three based on funding and cost constraints.

[1] A variant design is possible in which fixed bundle pairs are assigned to each positioner in order to provide a constant set of sky-object pairs.

[2] The ADC is oversized at 11 arcmin in diameter to accommodate guide and wavefront sensor cameras at the field perimeter.

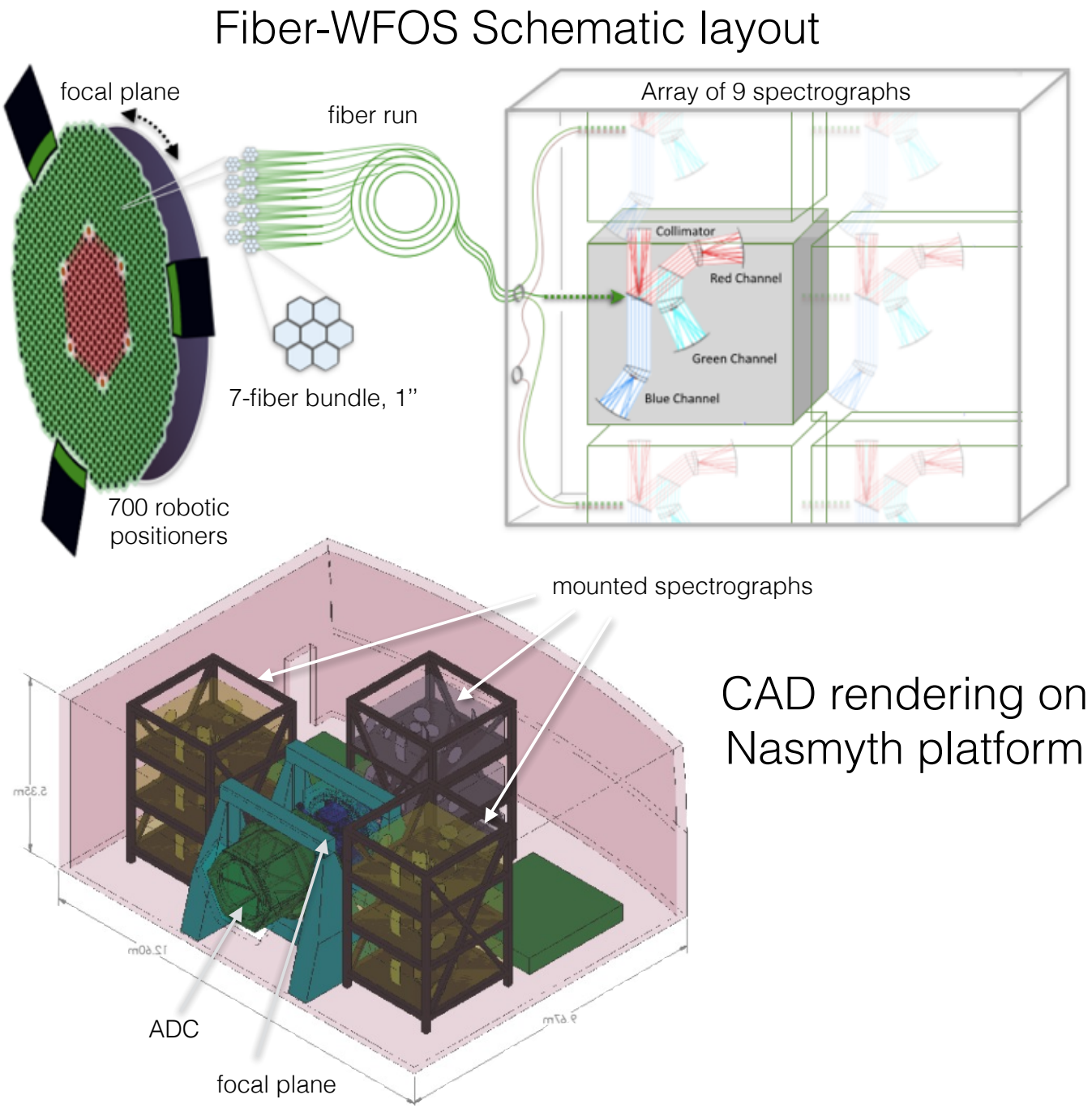

Figure 5: Fiber-WFOS schematic layout (top) and CAD rendering on the TMT Nasmyth platform. Light from TMT enters from the left. Nine spectrographs are mounted near the focal plane system to reduce the fiber run distance.

The relatively large fiber actuator size and minimal cost of deploying an alternative fiber system on the same actuators allows for flexibility in how the instrument will be used. This is particularity valuable in the context of GLAO were 7-fiber collectors could be augmented with larger 127-fiber bundles to enable a GLAO multiplexed IFU mode feeding the same WFOS spectrograph. Even without GLAO, the collecting solid angle (over 340 arcsec^2) of deployed large IFUs offers interesting potential for sampling arcmin-scale objects. Other second generation TMT instruments considering fibers may also be able to fold into the same robotic focal plane.

4 Comparisons Between Design Concepts

Here we focus on comparisons of expected performance, scientific potential, cost, and risk between XChange-WFOS and Fiber-WFOS Stage-1, in which just 6 of 9 spectrographs is initially populated. We find that XChange-WFOS does an excellent job providing the desired set of capabilities that motivated earlier WFOS designs. It also provides flexibility from the point of view of custom slit masks and offers various upgrade paths for achieving higher spectral resolution ($R \sim 15000$). Fiber-WFOS is less flexible in terms of spectral resolution but provides significantly greater information content at fixed exposure time, especially for samples of ∼100 objects or more. It opens new scientific opportunities with spatially-resolved spectroscopy and provides faster acquisition and characterization of transient discoveries. Developments in fiber instrument technology over the last 10 years have addressed limitations in previous fiber instruments. It is now possible to demonstrate that high-precision and faint optical spectroscopy with fibers is possible. Our work on this topic is summarized in a separate section, Section 5.

4.1 Information content "volume" and survey speed

Summary: Accounting for multiplex, resolution, throughput, and wavelength coverage, Fiber-WFOS gathers significantly more information per unit exposure time than XChange-WFOS at levels of a factor-of-few to more than an order-of-magnitude, depending on wavelength and resolution. This is made possible by the ability of Fiber-WFOS to reformat the focal plane and spectroscopically sample it at higher density over a larger field of view. With more detector pixels devoted to object flux (instead of sky), and no over-sampling, Fiber-WFOS Stage-1 can record ∼10 times the volume of information with only ∼4 times the number of detector pixels as XChange-WFOS. Note that low-resolution with Fiber-WFOS Stage-1 is achieved through spectral smoothing (see Section B.4).

In broad terms, the capabilities of the two instrument designs can be considered in terms of the "volume" of information that can be obtained by either instrument over the same exposure time. For a fixed sample of objects and desired amount of information, this information volume is equivalent to survey speed. Different dimensions in this volume may matter more or less to different science cases, but to first order, we are interested in the overall multiplex, throughput, instantaneous wavelength coverage, and spectral resolution achieved by each concept.

Multiplying these together, Figure 6 shows that Fiber-WFOS Stage-1 provides several factors to more than order-of-magnitude gains in information volume per unit time compared to XChange-WFOS, even when target efficiencies for sky-nodding observations are accounted for (bottom table). These allocation efficiencies are computed for Fiber-WFOS Stage-1 using simulations assuming a source density of 10 arcmin^{-2} (appropriate for faint high-z galaxies) and assigning individual bundles (from different positioners) to either object or sky to make object-sky pairs that are separated by a constant nod distance. The simulations show that 95% of bundles can be assigned to these object-sky pairs (see Fiber-WFOS: Target Allocation). The targeting efficiency would be similar if two bundles, i.e., if object-sky pairs, were instead affixed to each separate positioner. For sky-nodding with XChange-WFOS, we make an optimistic assumption that sources will be nodded 1″ along 5″-long slits and that the number of objects that can be allocated to slits is 65% of the maximum possible number of slits. Note that mask and slit assignment

Instrument Information Volume

	Resolution (mid channel)	Max multiplex	Instaneous bandpass (nm)	Throughput @320 nm	Throughput @900 nm	Data volume at @320 nm	Normalized volume @320 nm	Data volume at @900 nm	Normalized volume @900 nm
XChange-WFOS	1500	91	690	0.38	0.6	35790300	1.0	56511000	1.0
Fiber-WFOS	1500	700	690	0.33	0.55	239085000	6.7	398475000	7.1
Fiber-WFOS Lite	1500	468	690	0.33	0.55	159845400	4.5	266409000	4.7
XChange-WFOS	5000	91	245	0.30	0.64	33442500	1.0	71344000	1.0
Fiber-WFOS	5000	700	690	0.33	0.55	796950000	23.8	1328250000	18.6
Fiber-WFOS Lite	5000	468	690	0.33	0.55	532818000	15.9	888030000	12.4
XChange-WFOS	3500	91	530	0.37	0.53	62457850	1.0	89466650	1.0
Fiber-WFOS	3500	700	690	0.33	0.55	557865000	8.9	929775000	10.4
Fiber-WFOS Lite	3500	468	690	0.33	0.55	372972600	6.0	621621000	6.9

Information volume with sky-nod targeting efficiency

	Resolution (mid channel)	Allocated targets	Instaneous bandpass (nm)	Throughput @320 nm	Throughput @900 nm	Data volume at @320 nm	Normalized volume @320 nm	Data volume at @900 nm	Normalized volume @900 nm
XChange-WFOS	1500	60	690	0.38	0.6	23598000	1.0	37260000	1.0
Fiber-WFOS Lite	1500	233	690	0.33	0.55	79581150	3.4	132635250	3.6
XChange-WFOS	5000	60	245	0.3	0.64	22050000	1.0	47040000	1.0
Fiber-WFOS Lite	5000	233	690	0.33	0.55	265270500	12.0	442117500	9.4
XChange-WFOS	3500	60	530	0.37	0.53	41181000	1.0	58989000	1.0
Fiber-WFOS Lite	3500	233	690	0.33	0.55	185689350	4.5	309482250	5.2

Figure 6: The "volume" of information obtained by each instrument concept for the same exposure time. Here, *volume* is taken as the product of resolution, multiplex, instantaneous bandpass (wavelength range), and throughput (evaluated at two wavelength locations). The upper table considers the maximum possible multiplex, while the lower table assumes sky-nod pairs have been defined for both instruments, yielding an estimate for the number of successfully allocated targets. Even with half of fiber bundles reserved for sky, the normalized volume columns indicate that Fiber-WFOS Stage-1 provides 4–10 times the information volume of XChange-WFOS depending on resolution and wavelength. The gains come from the greater multiplex and full-band instantaneous wavelength coverage.

calculations in the MOBIE OCDD assumed 4″-wide slits (without sky nodding) and found that 60% of the maximum slit number could be assigned to targets. A 0.5″ gap between slits is included for separating spectral traces.

With these target efficiency assumptions and optimized XChange-WFOS slits, at 320 nm and $R \sim 5000$, Fiber-WFOS Stage-1 gathers 12 times the information content of XChange-WFOS. At $R \sim 1500$ and $R \sim 3500$, the gain is a factor of 3–4. Similar results are seen at 900 nm.

Nod-and-shuffle schemes would reduce the number of allocated targets in Figure 7 by a factor of ∼2 for both instruments. As discussed in Section B.3, for a 1 min exposure time, the read noise error contribution is modestly worse in Fiber-WFOS than it is in XChange-WFOS. If such short exposures are desired for temporal sky sampling, it is likely that nod-and-shuffle would be necessary for both Fiber and XChange options.

4.2 Throughput

We estimate end-to-end throughput curves that include all system components except the telescope and atmosphere (Figure 8). Aperture losses are not included because Fiber-WFOS bundles subtend ≈0.7 arcsec^2, similar to a typical object-extraction region for a 0.75″-wide XChange-WFOS slit. A workbook with assumptions on throughput losses used in Figure 8 can be made available. Fiber-WFOS remains competitive with XChange-WFOS because the throughput is optimized over 4 wavelength channels and because the fixed format of fiber spectra on the CCDs allows for wavelength-optimized detector coatings. Fiber-WFOS meets the 30% throughput requirement at 310 nm, while a steep UV efficiency fall-off in previous VPH gratings yields a lower value for XChange-WFOS if the manufacturing techniques used for the KCWI gratings are assumed. These techniques are being improved and enhanced UV VPH gratings should be forthcoming—their positive impact is apparent in the upper curves of Figure 4). XChange-WFOS may also be able to take advantage of the FSE gratings that Fiber-WFOS utilizes to achieve high UV throughput.

The assumptions for the two concepts in Figure 8 are conservative and based on as-built technology. For a sense of how XChange-WFOS throughput varies under different assumptions and spectral modes, please see XChange-WFOS: Optical and Structural Layout and Figure 4). For example, at $R \sim 1500$, the peak XChange-WFOS throughput improves by a factor of ∼1.16 over that obtained for the super-blaze at $R \sim 5000$.

4.3 Spectral Mode Flexibility

A benefit of XChange-WFOS is its flexibility in configuring separate spectral modes in the two wavelength channels. The spectral resolution in Fiber-WFOS is fixed at $R \sim 5000$, although one benefits in S/N by smoothing to lower resolution (see Section B.4). For some science programs, there will be observed-frame wavelength regions of particular interest that can be captured in 1 spectral mode of XChange-WFOS. In this case, the information gathering advantage of Fiber-WFOS Stage-1 reaches its minimum value of 7.5 at 320 nm and 4.0 at 900 nm (assuming sky nodding, see Figure 6) independent of spectral resolution.

The ability to set up one channel at low resolution and the other at higher resolution is also helpful. For Fiber-WFOS, when the data are read-noise limited (Section B.2) the S/N boost from smoothing is a factor 0.78 lower than the equivalent S/N boost from switching to low-resolution mode in XChange-WFOS. At 320 nm (read noise is likely to matter most at blue wavelengths), this effect lowers the Fiber-WFOS Stage-1 advantage from 7.5 to 4.5.

Perhaps the greatest advantage to the spectral flexibility of XChange-WFOS is the ability to add future custom gratings that may provide higher spectral resolution over important, if narrower, wavelength ranges.

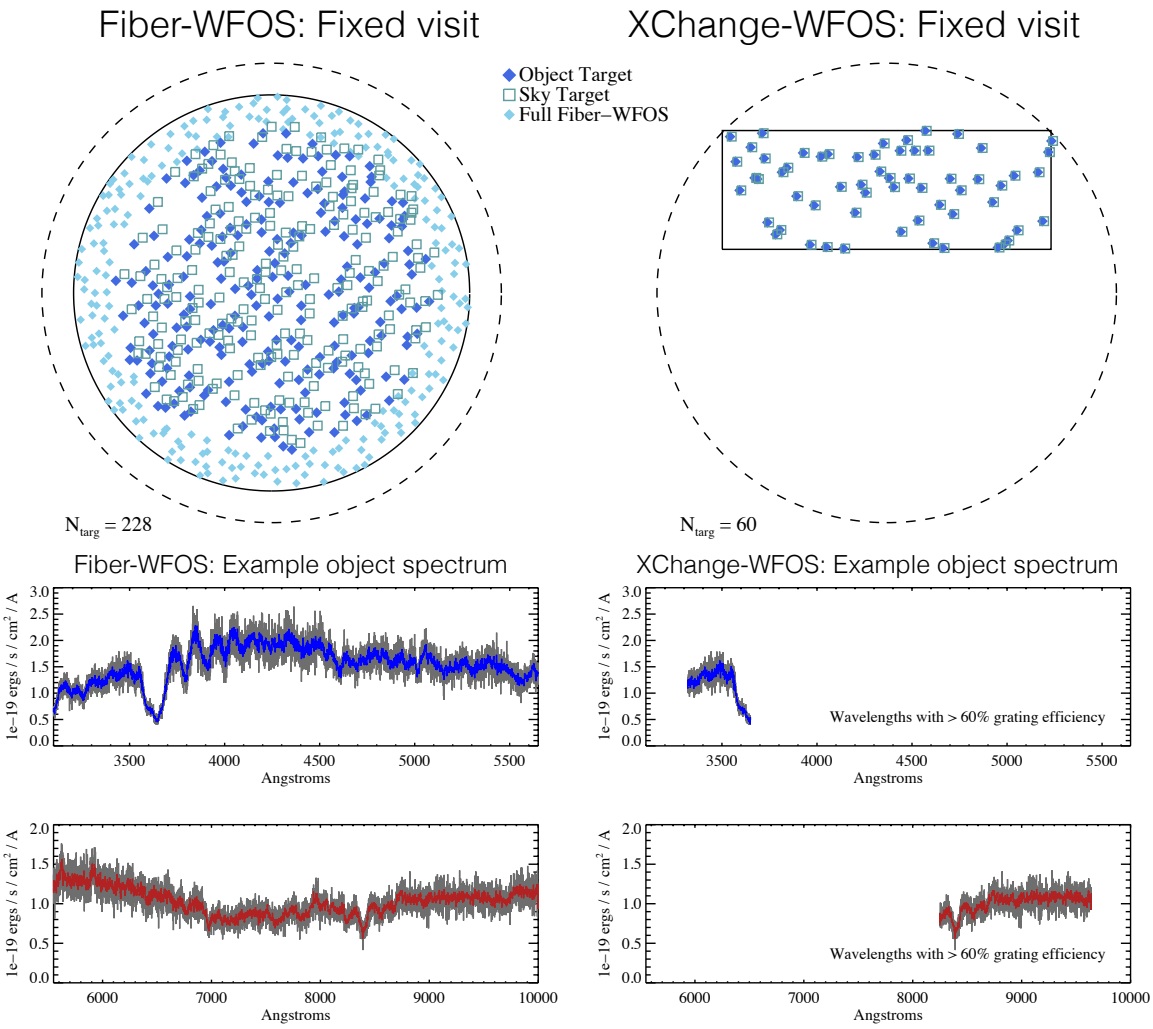

Figure 7: Visual representation of the information gathering power in sky-nodding mode of both concepts (see tables in Figure 6). At the top, the TMT field at a diameter of 12′ (dashed circle) and 10′ (solid circle) is indicated along with allocated targets (filled diamonds) and sky positions (open squares). Lighter and smaller filled diamonds show the additional bundles that would be available with the full Fiber-WFOS complement. For a single visit configuration (i.e., fixed targets and spectral mode) over a multi-hour integration, an example galaxy spectrum (24.5 AB at $z = 2.0$) at $R \sim 5000$ from one of the observed targets is shown (at S/N ∼10 per resolution element, the per-pixel noise level is apparent in grey; thicker lines have been smoothed by 6 pixels). For XChange-WFOS, only those wavelengths where the grating efficiency is $> 60\%$ are shown. Multiple visits with XChange-WFOS in different spectral modes are needed to cover a wider wavelength range at this resolution.

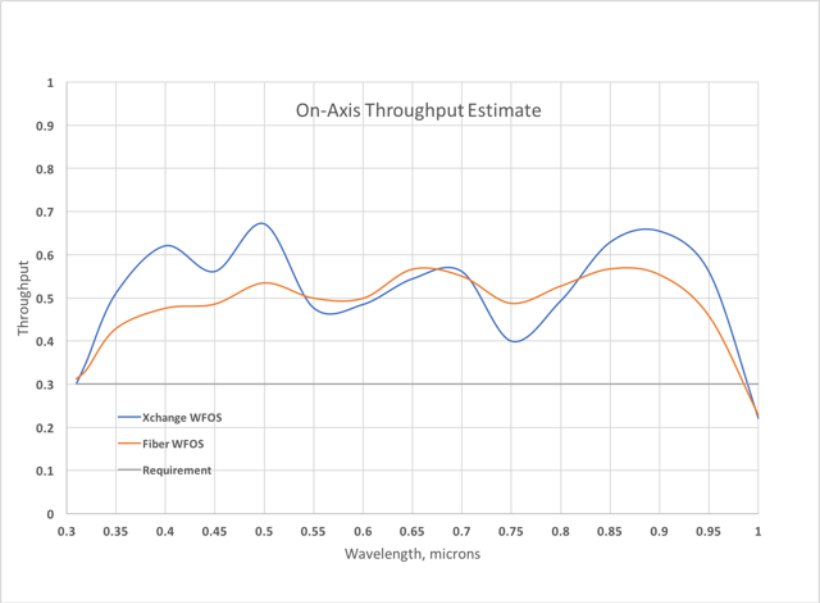

Figure 8: Throughput curve comparison for Fiber-WFOS and XChange-WFOS at $R \sim 5000$ with consistent assumptions, including a conservative 0.5% AR coating loss per surface. The assumptions used for XChange-WFOS are similar to those in Figure 4. The requirement was to have greater than 30% end-to-end throughput at all wavelengths.

4.4 Requirements, Capabilities, and Scientific Potential

4.4.1 Meeting Requirements

Both Fiber-WFOS Stage-1 and XChange-WFOS provide the core capabilities long desired for WFOS and meet the majority of high-level WFOS Observatory Architecture Requirements (see Appendix A). There are three exceptions to point out.

First, at the beginning of the current design phase, it was recognized that the initial concepts under study (Fiber-WFOS and Slicer-WFOS) did not allow for imaging modes. Supported by the recommendation from the WFOS Science Committee to de-prioritize imaging in light of the scientific landscape in 2030 (see the OMDR Science Definition and Design Drivers report), the imaging requirement was dropped. The advent of XChange-WFOS restores an imaging capability over its full 8.3 × 3 arcmin field. Fiber-WFOS does not provide direct imaging, but does enable imaging spectroscopy with flexibly sized fiber bundles over a total collecting area of 350 arcsec^2.

Expected technological advances should enable XChange-WFOS to meet the 30% throughput requirement blueward of 325 nm (see XChange-WFOS: Optical and Structural Layout). Regarding read noise, Fiber-WFOS is also somewhat below the background-limited threshold for 1 minute exposures and 3 e$^-$ read noise per pixel at blue wavelengths (see Section B.2).

4.4.2 Instrument Capabilities

We consider several specific aspects of the instrument capabilities.

- **Spatial Sampling:** The Fiber-WFOS fiber bundles are small integral field units (IFUs) and thus provide valuable spatial information that can be used to construct a map of the PSF across the focal plane and to recover spatial information about extended sources. The position angles (PAs) of galaxy major axes could be recovered and sampled, for example, at arbitrary sky angle, whereas slits with XChange-WFOS would be limited to ±30°. Dithered Fiber-WFOS observations would provide spatial sampling of the PSF at 0.1″ (see Law et al., 2015).

- **Spectrophotometric Flux Calibration:** A PSF model afforded by targeting ∼10 stars within every Fiber-WFOS pointing would enable an accurate determination of aperture loss across the field. By color-selecting these stars to have certain stellar types (e.g., F-type) theoretical spectral energy distributions can be predicted, providing spectrophotometric flux calibrations for all Fiber-WFOS targets at an expected relative precision of 5% between 3727 Å and 6583 Å (Yan et al., 2016). The typical flux calibration precision for slit-mask observations is ∼20%.

- **Instant Spectroscopy of Transient Sources:** With Fiber-WFOS Stage-1, a single over-sized 37-fiber bundle (subtending 3″) would be fixed near the field center. Transient sources could be followed up instantly with this central IFU, requiring no instrument configuration changes and ensuring that the object is captured despite any pointing errors.

- **Aperture Flexibility:** XChange-WFOS offers flexible slitmask design. Slits may be elongated for certain targets or made wider or narrower should the observer wish to trade collected flux against spectral resolution[3].

  Aperture adjustment with Fiber-WFOS is more limited and cannot be used to change spectral resolution. Here desired flexibility should be built into the design. Fiber-WFOS Stage-1 baselines 468 7-fiber bundles, but incorporating a fraction of larger bundles (19-fiber bundles would each subtend 1.7″, 61-fiber bundles would subtend 3″) may be desirable and should be studied further based on relevant science cases.

- **Integral-field (IFU) Resolved Spectroscopy:** At modest cost (2–5% of the total budget) a single image-slicer IFU could be added to XChange-WFOS. For the same price with Fiber-WFOS, a second observing mode could be enabled in which the fibers are distributed into, e.g., 38 deployable IFUs, each with 127 fibers. Behind a ground-layer adaptive optics (GLAO) system, each of these 127-fiber bundles would subtend ∼1″ and provide spatial sampling of the ∼0.3″ FWHM GLAO PSF (evaluated at 600 nm) at a spatial scale of 0.1″. For natural seeing applications, the IFU configuration could be designed to provide larger bundles for imaging spectroscopy over arcsec scales across sources that extend throughout the field (e.g., galaxy clusters, nearby dwarf galaxies, Ly-α nebulae). The total collecting solid angle would be 346 arcsec^2 with the full Fiber-WFOS, similar to KCWI's 20″ × 20″ field. With associated collectors and fibers for the IFU and mini-bundle modes installed simultaneously and sharing positioners, a pseudo-slit exchange mechanism would enable observers to switch between to the desired observing mode.

- **Imaging:** XChange-WFOS provides direct imaging of its 8.3′ × 3′ field. There is no direct imaging in Fiber-WFOS, but deployed fiber bundles enable imaging spectroscopy over a substantial solid angle (230 arcsec^2 for Fiber-WFOS Stage-1 and 346 arcsec^2 for full Fiber-WFOS).

4.4.3 WFOS Core Science and Upgrade Potential

By meeting the majority of basic high-level requirements, both instrument concepts address the four core WFOS science cases identified in the OMDR Science Definition and Design Drivers document. A few notes are worth making:

- **IGM Tomography at $z \sim 2$:** The ability to characterize high-redshift galaxies and their intervening gaseous environment is a top priority and major design driver for WFOS. The MOBIE Operational Concepts Definition Document (MOBIE OCDD) defined an ambitious IGM tomography program to obtain spectroscopy for ∼40k galaxies over 160 TMT nights. With Fiber-WFOS, the same program could be accomplished in ∼20 nights.

[3]Because of the small pixel size in XChange-WFOS, slits as narrow as 0.2″ would be adequately sampled

- **Stellar Observations:** The multiplex and field-of-view of XChange-WFOS makes it well suited to studying the stellar populations and kinematics of dwarf galaxies at $D > 1$ Mpc, portions of M31, and globular clusters (see OMDR Science Definition and Design Drivers report). Fiber-WFOS would make WFOS more competitive in the context of forthcoming highly multiplexed spectrographs on 8m class and smaller telescopes (e.g., PFS, MOONS, 4MOST) for scientific programs studying local-group galaxies. Survey programs in M31, in particular, could be carried out ∼10 times faster with Fiber-WFOS Stage-1 than XChange-WFOS. In addition, Milky Way science programs (e.g., halo stars) that are too low-density to be compelling with XChange-WFOS can interleave their targets into wide-field programs with Fiber-WFOS.

- **Resolved galaxies at $z \sim 1$:** Even in natural seeing, spatially-resolved spectroscopy is a useful tool for studying the internal structure of distant galaxies. With the potential for a GLAO-corrected ∼0.3″ FWHM (at 600 nm), resolved spectroscopy is much more compelling as physical scales relevant to galaxy evolution (∼2 kpc) become accessible at $z \sim 1$. Only with the collecting area of ELTs can a sufficient continuum S/N be obtained for $z \sim 1$ stellar populations resolved at such spatial scales. The multiplexed large-IFU mode behind GLAO with Fiber-WFOS would open up significant new science capacity for TMT. XChange-WFOS would be less compelling but would still provide interesting spatially-resolved information along each slit (e.g., rotation curves), for smaller samples.

- **Transient Followup:** Both instruments would be able to rapidly follow up transient discoveries. With a fixed and over-sized central fiber-bundle, Fiber-WFOS would provide somewhat faster target acquisition without pointing error concerns. Its full wavelength coverage at $R \sim 5000$ may be an advantage for source identification and previously-defined background target catalogs could ensure that all bundles are collecting scientifically valuable information on other targets in the field, regardless of where in the sky the transient of interest is located.

  For XChange-WFOS, several minutes would be required if the spectral mode that XChange-WFOS was previously in had to be reconfigured for a target-of-opportunity observation. Several separate exposures, with 2–3 minute reconfiguration times in between, would also be required to cover a large wavelength range with XChange-WFOS at $R \sim 5000$. If a specific spectral feature at a given observed-frame wavelength were the top priority, however, XChange-WFOS could be outfitted with a custom grating to capture this feature at a desired resolution.

- **Dark Energy Science:** The multiplex capability of Fiber-WFOS combined with TMT's collecting area would make it the most powerful instrument for spectroscopic training of the photometric redshifts used in upcoming dark energy experiments with facilities like LSST and WFIRST. The 75% complete LSST photo-z training program described in Newman et al. (2015) could be completed in ∼50 nights with the full Fiber-WFOS. Despite the high monetary value of a single TMT night, such a Fiber-WFOS program would carry a cheaper overall price tag (by a factor of ∼2) than the same program consuming more than a year of continuous observing with Subaru-PFS. In practice, it would make sense to prioritize the fainter targets for TMT, which would come online as LSST begins reaching full depth, but the promise of Fiber-WFOS in this area has motivated interest in WFOS from DOE (Dawson et al., 2018, Fiber-WFOS is mentioned in Section 2.1) and NASA-WFIRST, which has sent a letter of interest in Fiber-WFOS to the TMT Project Office.

The scientific potential of both instrument concepts can also be compared in terms of possible upgrade paths that would provide a substantial scientific benefit. We consider two areas for upgrades that may be of interest. The first is reaching higher spectral resolution, of order $R \sim 15000$, especially for the identification of spectral features associated with specific elements in stellar sources. XChange-WFOS offers the best options here. With no upgrades required, XChange-WFOS can observe $R \sim 15000$ over the same wavelength range zones defined for the $R \sim 5000$ mode simply by cutting narrower slits (0.25″ instead of 0.75″) and accepting the resulting aperture losses. Behind GLAO, $R \sim 15000$ with narrow slits

is possible with much reduced aperture losses. Finally, a possible upgrade may be to add a Slicer-WFOS slicer module (or more than one) to XChange-WFOS so that high resolution can be achieved with no aperture loss (and without GLAO).

No simple upgrades to reach $R \sim 15000$ with Fiber-WFOS are possible, and this spectral resolution is not a benefit of GLAO in the fiber-based design (because the fiber size as seen by the spectrograph is fixed). To achieve high-resolution spectra, the best option for Fiber-WFOS would be to optimize some number of the fiber spectrographs for high-resolution (either in addition to or at the cost of the $R \sim 5000$ spectrographs) and interleave their corresponding bundles into the focal plane.

The second area for a possible upgrade is a redder wavelength limit, possibly exploiting emerging germanium CCD technology to reach 1.3 μm. The Fiber-WFOS spectrographs can be designed to anticipate this technology should it become available through an additional or upgraded near-IR channel. Given space limitations in XChange-WFOS, adding a third wavelength channel seems unworkable.

4.5 Risk Comparison

The WFOS team's assessment shows comparable levels of risk in both instrument concepts. There are few components in either design that have not previously been built at the required size or specifications. The most important scientific risk for Fiber-WFOS, the fiber systematics contribution to instrument stability and sky subtraction, has been exhaustively studied in this phase and is summarized in its own section (Section 5. A full register of risks can be found in the Risk Assessment.

4.5.1 Stray light

Both instrument designs offer pupil masking opportunities that can mitigate the impact of stray light. Baffles could be placed on gratings in the case of XChange-WFOS and within the bundle fore-optics for Fiber-WFOS.

4.6 Cost Comparison

By populating just 6 of 9 spectrographs, Fiber-WFOS Stage-1 is only modestly more expensive than XChange-WFOS. The fiber-based concept also has cost advantages because of its modularity. An upfront investment in design, engineering, and expertise is required for the first spectrographs, but their replicated nature means one can reap the benefits of this investment as future articles are built. The cost per spectrograph therefore decreases as more are built. The modularity also allows Fiber-WFOS to be built in phases according to budget constraints.

Detailed budgets are forthcoming. For Fiber-WFOS Stage-1, the budget is based on a bottoms-up assessment of the effort required for each subsystem, costs for similar instruments and vendor quotes for certain commercial off-the-shelf (COTS) items. The XChange-WFOS budget is based on scaling recent instrument developments, vendor quotes for the large optics, and comparison with the MOBIE cost estimates.

4.6.1 Fiber-WFOS: A Robotic Positioning Facility for TMT

An important fraction of the cost of Fiber-WFOS is the focal plane system and robotic positioners. Once complete, this system is capable of feeding other, future TMT instruments that would use fibers to collect light at the Nasmyth focal plane. Fiber-based versions of the High-Resolution Optical Spectrometer (HROS), the Infrared Multi-Object Spectrometer (IRMS), and other instruments could all make use of this focal plane facility.

5 Fiber Systematics and Sky Subtraction

Summary: The team has undertaken a comprehensive study of fiber systematics based on data from SDSS-MaNGA and other fiber instruments. The results are collected in a draft manuscript on the subject (Fiber Systematics and Sky Subtraction) and the spectra analyzed are made publicly available[4] on a website. The paper's key findings are an exposure-to-exposure per-fiber continuum variation of 0.1% due to changing fiber stresses at the level expected for Fiber-WFOS. Such variations are stochastic and beat down further with integration time, remaining at negligible levels for all integrations. The LSF FWHM varies at less than 1.6% as a result of changing fiber stresses, sufficient for limiting sky line residuals to an amplitude just above the Poisson limit. Bolstering these results are three on-sky demonstrations. A 13.5-hour MaNGA observation (Gu et al., 2017) with 19-fiber bundles reaches a continuum surface brightness 6.7 magnitudes below the sky background (a precision of 0.2%). And an analysis of all-sky fiber observations shows that even non-local sky subtraction can remove sky lines to nearly the Poisson limit when 50% of fibers are sampling sky. The MaNGA results are reassuring, especially because MaNGA was never intended to reach such high levels of precision. Finally, sky-only beam-switching observations with the Nasmyth-mounted VLT-GIRAFFE demonstrate 0.01% accuracy for a single fiber with 1 hour total integration time.

5.1 Background

For many astronomers, experience with fiber-based instruments built 10 to 20 years ago has given fibers a bad reputation for low throughput and poor stability that renders precision sky subtraction next to impossible. Many believe that fiber instruments can therefore only work for highly specialized surveys of bright sources (on small telescopes). Thankfully, this reputation is no longer accurate. Our understanding of what can limit fiber performance has dramatically improved in recent years, and new technology now allows us to take advantage of this knowledge. Many sections of the community are investing heavily in fiber instruments designed to go deep on large telescopes (e.g., Subaru-PFS), and ironically, the very high spectral resolution community (e.g., $R \sim 150,000$ for extrasolar planet hunting) is now building almost exclusively fiber-based spectrographs *because* of their proven ability to provide a more stable instrument response than a traditional slit-based instrument (e.g., Halverson et al., 2015).

The biggest problem with early-generation fiber instruments was the inability to control and mitigate focal ratio degradation (FRD), which simply describes an increase in the opening angle of the light cone output by fibers. Fibers can typically accept light at wide angles (f-numbers like f/2.3), but even if the telescope beam input is slower, bends, stresses, and telecentricity misalignment will tend to distribute some light to the widest angles allowed. The relative importance of this FRD effect is worse as the input beam gets slower. As a result, earlier fiber instruments with collimators designed to accept f/8 or slower missed significant fractions of output fiber flux. Perhaps worse, the throughput loss varied with time due to fiber motion or changes in the angular alignment with the chief ray. This is a key reason why SDSS has been successful as a fiber facility—it has a very fast telescope beam (f/5) which reduces the relative impact of FRD.

For modern fiber-based designs like Fiber-WFOS, the advent of microlens arrays combined with other fore-optics allow fiber injection at f/3, even if the telescope provides f/15. Modern designs also pay far more attention to maintaining telecentricity across the focal plane and ensuring that fibers experience the minimum stresses and motion possible. Telecom industry led improvements to fiber throughput (losses are typically 1% per meter in the UV and are otherwise negligible from the optical into the near-IR) have also been important.

The remaining question we have addressed in this phase (see below) is whether these improvements in fiber instrument technology are sufficient to provide the required high level of precision for background

[4] http://www.ucolick.org/~kbundy/fiber_stability/

subtraction of extremely faint objects with the TMT. We conclude from an extensive analysis that the answer is yes.

5.2 Fiber systematics in sky subtraction

The analysis of fiber stability and potential contributions from fiber systematics to sky foreground subtraction has been collected in a draft Fiber Systematics and Sky Subtraction manuscript. The topic has attracted interest outside of TMT as the analysis is relevant to other fiber-based designs on large telescopes.

The paper draft initially defines the problem of foreground subtraction and introduces a formalism for considering systematics of various methods (Section 2). While non-local sky subtraction remains the goal because it maximizes use of the instrument for targeting actual sources, this paper simplifies the problem by focusing on sky-nodding strategies (local sky subtraction).

In Section 3, the potential origins of systematic terms in fiber instruments are discussed. The essential problem is understanding how stable the throughput and line-spread function (LSF) remain for a given fiber as the instrument moves (due to field tracking) and the fiber experiences changes in stress. Significant variations between the short exposures (∼1 min) that would be used for sky-nodding would lead to systematic residuals and error terms, but Section 3 demonstrates that for a Nasmyth mounted instrument like Fiber-WFOS, the amount of fiber motion that occurs on the scale of a few minutes is very small. On this basis alone, one would expect any systematic terms to almost perfectly cancel between on-source and on-sky exposures.

Section 4 utilizes calibration data from SDSS-IV MaNGA to determine how much the changing stress states of fibers in an actual instrument affect the instrument response. Flat fields provide very S/N that allows continuum sensitivity to 0.1% precision levels, and different experimental tests can be used to isolate the impact of fibers on the throughput stability from other contributions in the high-flexure MaNGA/BOSS spectrographs. We find that for the same fiber experiencing stresses at a level expected for Fiber-WFOS over a ∼1 minute timescale, the overall throughput normalization varies stochastically at 0.1% from one exposure to the next. There is no evidence for drift or persistent residuals between exposure pairs. Thus, with the combination of many exposure pairs in a sky-nodding sequence (or the use of many separate fibers in a non-local subtraction scheme), the additional systematic noise contribution beats down with time. Even without this, however, it is negligible at all exposure times. Interestingly, the worst possible variations that can be engineered in the MaNGA instrument (by comparing wildly different fiber stress states) still only contribute an additional error term at the 1–2% level per exposure pair. With exposure averaging, even this systematic contribution would be acceptable to WFOS.

Figure 9 shows this by including the contributions of fiber systematics in the estimated S/N increase with integration time for a single target observed with sky-nodding observations with Fiber-WFOS. With the expected Fiber-WFOS systematics, the final S/N (dashed blue line) and that calculated from Poisson noise only (thick grey line) are indistinguishable. Even when the maximum level of continuum fiber systematics observed in MaNGA are included (dotted grey line) the S/N degrades by just ∼6%. Even these data would be considered Poisson-limited. The green line shows the improved S/N at fixed exposure time achieved with non-local sky subtraction in which source flux is collected 100% of the time (as opposed to half of the time with sky-nodding). We assume that a noise term has been introduced into an otherwise perfect sky model by inserting the maximum variations observed by MaNGA into the ∼70 fibers used to construct the model. This is equivalent to assuming that the instrument is perfectly calibrated but experiences the worst possible fiber variations over the course of the integration.

A related test shows that the instrumental line width varies by 1.6% between exposures with the same fiber. This variation should ensure excellent sky line subtraction, but this result is subject to more uncertainty given the difficulty of measuring line widths for relatively sparse arc lines. Instead, the most convincing argument regarding sky line subtraction comes from an actual demonstration shown in Section 5.2. Here MaNGA all-sky data is reduced in a way that uses 50% of the fibers to sample the sky. Near Poisson-limited subtraction is achieved at the reddest wavelengths (near 950 nm) where skylines are particularly strong, despite the fact that the method is still non-local (see Figure 13 in the Fiber Systematics

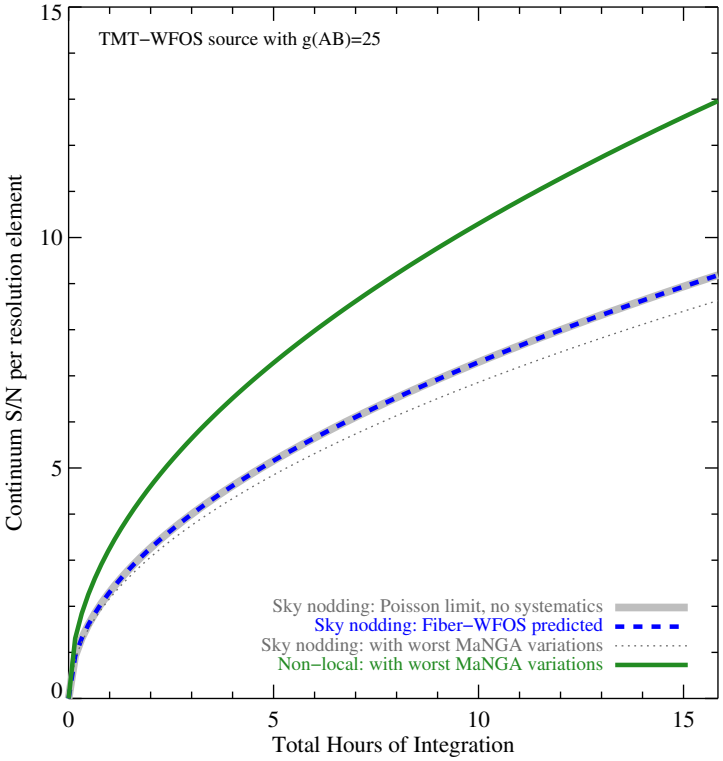

Figure 9: Impact of estimated fiber systematic errors on the obtained Fiber-WFOS signal-to-noise from long sky-nodding observations. The final S/N (dashed blue line) including the expected level of continuum fiber systematics and that calculated from Poisson noise only (thick grey line) are indistinguishable. Even the worst-case variations that can be engineered from the MaNGA data provide an acceptable degradation in S/N (dotted line). The green line indicates the improved S/N at fixed integration time from using non-local sky subtraction to collect source flux 100% of the time.

and Sky Subtraction). This not only demonstrates that a fiber-instrument employing sky-nodding would achieve exquisite skyline subtraction but argues that improvements to psuedo-slits and an increase in sky sampling fibers could achieve near-perfect results with non-local techniques[5].

Section 5.3 presents a science demonstration of background precision at the level of 0.2% achieved with 13.5-hour MaNGA observations in the Coma cluster (Gu et al., 2017). This result is impressive because MaNGA was never designed to achieve such high precision. The reason that this result is relevant to TMT despite coming from a 2.5 m telescope is the fact that the MaNGA data was collected over a larger solid angle, 59.7 arcsec^2 for an integrated 19-fiber MaNGA bundle versus 0.7 arcsec^2 for an integrated 7-fiber Fiber-WFOS bundle. So while the integrated flux of faint sources on TMT would be much smaller, the desired surface brightness level below the sky foreground is comparable. Either way, 0.1–0.2% precision is required and the impact of fiber systematics is similar. In the MaNGA Coma data, these systematics are demonstrably low in order to allow the observations to reach such depths in the given exposure time. Note that the MaNGA Coma observations were reduced primarily with non-local sky subtraction with an additional correction from sky-nods that consumed one-third of the total integration time.

Finally we reanalyze VLT-GIRAFFE all-sky observations in Section 5.1 to confirm a mean residual of 0.01% using beam-switching techniques (Rodrigues et al., 2012).

[5]With the assumption of a high-performing calibration system.

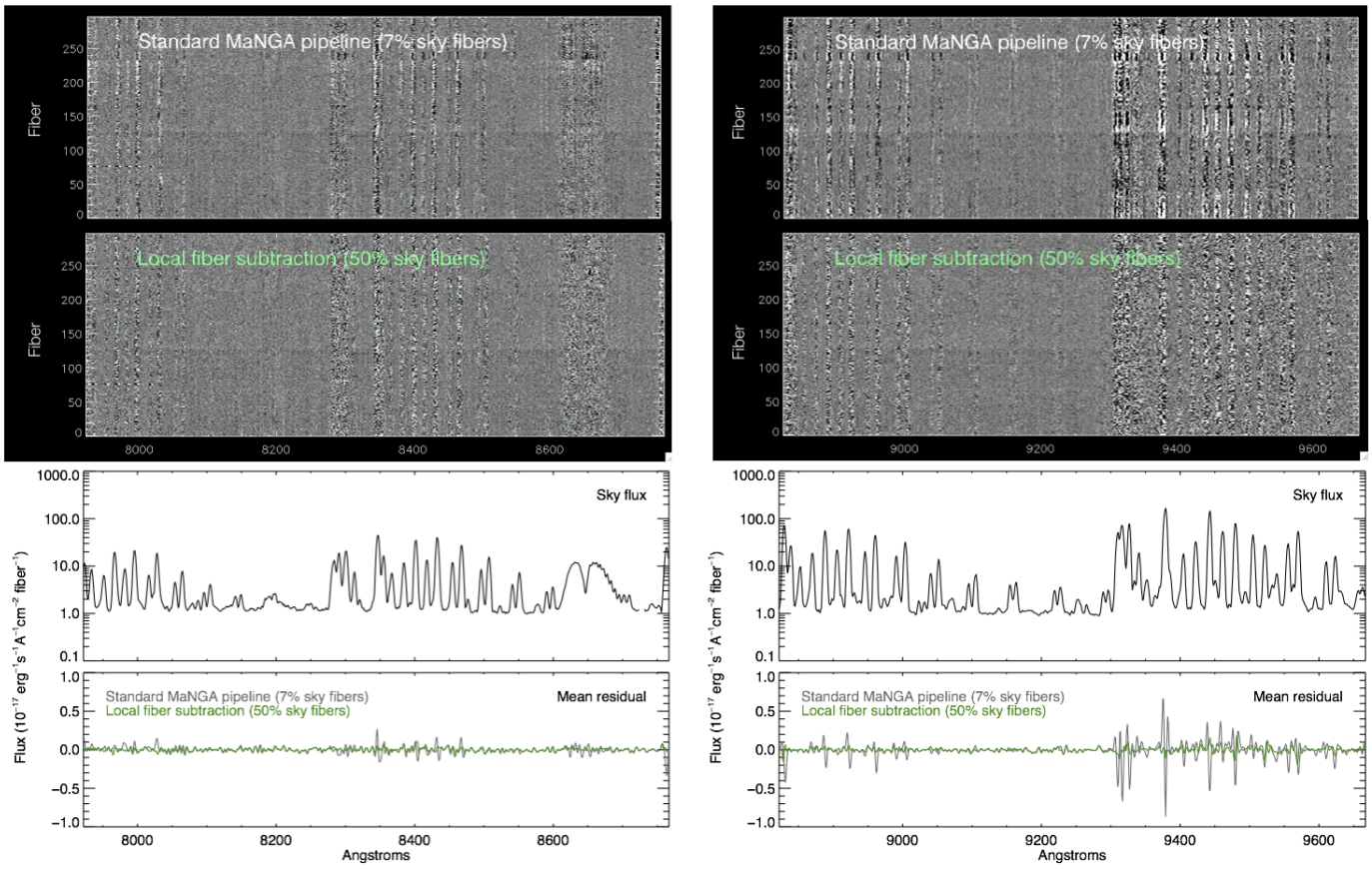

Figure 10: Pseudo-local subtraction of sky lines in MaNGA. The "images" in the upper panels are stacks of reduced and wavelength-rectified fiber spectra, where each row displays the 1D spectrum from a different fiber. The result in two red wavelength regions (left and right columns) for the standard pipeline output is shown in the upper panels. Systematic residuals near bright sky lines are apparent. A pseudo-local approach (2nd row of images) where the non-local sky sampling is increased to 50% of available fibers shows significant improvement. The mean sky flux and mean residual flux among this set of nearly 300 fibers is shown in the bottom panels.

6 WFOS Team Recommendation

Our recommendation is that Fiber-WFOS be pursued in the next design phase with a focus on further risk reduction in preparation for a full Conceptual Design Review (CoDR) in Fall 2019. Meanwhile, we recommend maintaining XChange-WFOS as a viable back-up option should the outcome of CoDR find an increased risk assessment for Fiber-WFOS or reveal new problems. The Fall 2019 timing would also allow initial performance assessments from DESI and PFS, major fiber-based facilities that will emerge from commissioning next year.

With this attention to retiring Fiber-WFOS risks, we will focus on three key items in the next phase:

1. **Sky-subtraction systematics.** A fiber test-stand apparatus capable of simulating and testing the impact of fiber stresses expected in Fiber-WFOS on the near and far-field fiber output so that these lab data can be tied to and used to validate the on-sky experiments described in Section 5.

2. **Bundle fore-optics.** Prototyping of the microlens array and fiber bundle fore-optics. This will allow a reduction in risk for manufacturing and assembly of these subsystems.

3. **Instrument calibration.** Study illumination sources and other aspects of the flat-field and arc lamp calibration systems developed for PFS and DESI. Produce a complete design for WFOS. An accurate calibration system would allow Fiber-WFOS to benefit from non-local sky subtraction, a high priority because it roughly doubles efficiency and obviates the need for short time sampling of the sky background.

Appendices

A Observatory Architecture Requirements

These high-level WFOS requirements have been updated for this phase and are under change-request.

[REQ-1-OAD-3300] In seeing limited mode, the image jitter resulting from the WFOS rotator shall be less than 33mas RMS.

[REQ-1-OAD-3306] WFOS shall provide atmospheric dispersion correction.

[REQ-1-OAD-3310] WFOS shall provide a LOWFS (Low order wavefront sensor) to supply active optics feedback signals.

[REQ-1-OAD-3322] WFOS shall provide internal baffling.

[REQ-1-OAD-3324] The WFOS wavelength range shall be 0.31 - 1.0 μm.

[REQ-1-OAD-3328] WFOS, in Spectroscopy Mode, shall have an image quality less than 0.2 arcsec FWHM at every wavelength, not including contributions from the telescope or the atmosphere.

[REQ-1-OAD-3330] The WFOS Field of View shall be >25arcmin^2

[REQ-1-OAD-3332] WFOS shall provide spectra of at least 20 objects at medium resolution (i.e., R 4500), and of at least 70 objects at low resolution (i.e., R 1500), assuming best-case on-sky locations of targets.

[REQ-1-OAD-3334] WFOS shall have a Spatial Sampling <0.15 arc-sec per pixel, goal <0.1 arcsec.

[REQ-1-OAD-3336] WFOS shall provide a median spectral resolution of at least R=4000, with the minimum spectral resolution in any broadband channel greater than R=3500.

[REQ-1-OAD-3338] WFOS, in Spectroscopy Mode, shall have a throughput of >30% from 0.31 - 1.0 μm, not including the telescope.

[REQ-1-OAD-3340] WFOS spectra shall be photon noise limited for all exposure times >60 sec.

[REQ-1-OAD-3341] WFOS background subtraction systematics shall degrade the total noise by less than 10% compared to photon noise for total exposure times as long as 100 Ksec.

[REQ-1-OAD-3342] WFOS shall have a gravity flexure due to instrument rotation at a level less than 0.15 arc-sec at the detector.

[REQ-1-OAD-3344] WFOS shall support short (¡ 3 minutes once telescope is in position) field acquisition for multi-object spectroscopy.

[REQ-1-OAD-3346] WFOS shall support fast (¡ 1 min) spectroscopic acquisition of single targets

[REQ-1-OAD-3348] A goal is to provide enhanced image quality using Ground Layer Adaptive Optics, over the full wavelength range, and the full field of the spectrograph.

B Additional Fiber-WFOS Considerations

B.1 Multiplex and Collecting Options

The primary gain of using fibers is a dramatic increase in multiplex (by many factors) without a loss in spectral resolution or wavelength coverage. This gain is possible for two reasons. First, collecting fibers are allowed to densely sample targets in both spatial dimensions, whereas slits cannot overlap in the dispersion direction. The overall sampling of the sources in the focal plane increases with fibers. Second, in a typical exposure multi-object slit-based instruments collect more blank sky flux than object flux, since objects within slits must be flanked by a significant stretch of sky pixels on either side. Fiber instruments can be optimized to collect more source flux. Finally, in the case of Fiber-WFOS Stage-1, approximately 4 times the number of pixels is used compared to XChange-WFOS.

B.2 Read Noise

Integrating the full solid angle subtended by a 7-fiber bundle, at $R \sim 5000$, the sky background[6] photon count rate is 200 min^{-1} per wavelength pixel at $\lambda \approx 4000$ Å.

This count rate is separated into 7 fibers. The spatial output profile of each fiber is Gaussian with a FWHM spanning ∼3 pixel columns of the CCD. We can roughly estimate the ratio of read noise to the Poisson sky noise background by considering two cases. If the fiber spatial profile was flat (instead of Gaussian), the total counts would be spread equally over 21 columns, giving a CDD per-pixel count rate of $S_p = 200/21 = 9.5$ photons min^{-1}. If we instead concentrate the flux in the central columns, the pixel count rate is $S_p = 200/7 = 28.6$ photons min^{-1}. Given a read noise, σ_R, the total variance per pixel (including both photon shot noise and read noise) is $\sigma_{tot}^2 = S + \sigma_R^2$. The ratio of the shot noise only to the total noise is

$$\frac{\sigma_{tot}}{\sigma_{shot}} = \sqrt{1 + \frac{\sigma_R^2}{S_p}} \quad (1)$$

where "background-limited" is often defined as $\sigma_{tot}/\sigma_{shot} < 1.1$, that is, the read noise contribution should not degrade the total error by more than 10%. In the two cases above, $\sigma_{tot}/\sigma_{shot}$ ranges from 1.40–1.14 for 1-minute exposures. Carrying out a Gaussian fit to the spatial profile (as is standard for fiber data

[6]Taken from the 50% median dark (±7 days from new moon, V(AB)=20.8 mag arcsec^{-2}) sky spectrum at Mauna Kea from the Gemini Website. At ∼4000 Å, the sky background on the darkest nights will be 3.5 times fainter.

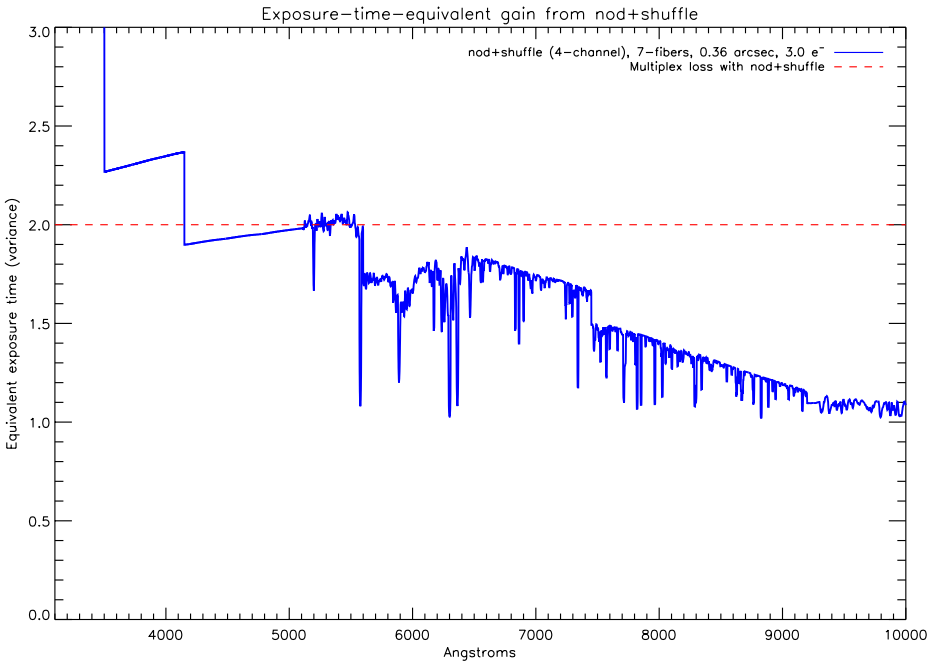

Figure 11: The exposure-time benefit of nod-and-shuffle observing (blue line) compared to the associated factor of 2 loss in multiplex (red dashed line). This figure is based on total noise estimates for an 8-hour on-source integration. If a given observing program makes maximum use of the available Fiber-WFOS multiplex, the overall observing speed at mid-to-redder wavelengths is faster when short exposures are read-out, even though the data would suffer a read noise penalty. This is not the case at the bluest wavelengths, a statement that strengthens on the darkest nights (when the sky background drops by a factor 3–4 compared to what is assumed here).

reduction) reduces the read noise penalty further ($\sigma_{tot}/\sigma_{shot} = 1.12$ at 5000 Å and $\sigma_{tot}/\sigma_{shot} = 1.17$ at 3100 Å), but even with spatial profile fitting, such short exposures with Fiber-WFOS are not quite background-limited. Exposures of 2–3 minutes would enter the background-limited regime. These exposures times may represent acceptable time sampling of sky variations in the sky-line-free blue channels. They may not be suitable for sampling more rapid sky *line* variations at redder wavelengths, but the sky background at these wavelengths is a factor of ∼2 brighter, so shorter exposures will not suffer the same read noise penalty.

For the slit-based WFOS designs, the detector pixels over-sample the atmospheric PSF (pixel scale is ≈0.05 arcsec) allowing CCD binning during readout, but only to the extent that spectral curvature (and other distortions) can be mapped adequately. If 3-pixel binning is possible in the spatial direction and a typical faint source spans 0.75 arcsec then the 200 counts obtained in a 1-minute exposure would be spread over 5 binned columns. The value of $\sigma_{tot}/\sigma_{shot}$ in this case would be 1.11. Nod-and-shuffle schemes are therefore important for XChange-WFOS and Slicer-WFOS as well.

B.3 Nod-and-shuffle

In the simplest implementation, fast reads of sky-nodding observations incur a second read-noise penalty because the read noise also effects the sky-only exposures (which are then subtracted from on-source exposures). If ∼1 minute sky sampling with Fiber-WFOS is required, nod-and-shuffle strategies can overcome the read-noise penalty by storing, in specific non-illuminated CCD columns, the charge recorded from alternating sky and source exposures (see Glazebrook & Bland-Hawthorn, 2001). In this approach, telescope nods are coordinated with CCD charge shuffling so that sky and source photons build up on specific parts of the detector, obviating the need for read-out and enabling exposure times of arbitrary length. The

read-noise penalty can be completely avoided, but this comes at the cost of allocating ∼50% of the detector pixels for charge storage regions. Because these pixels could otherwise record data from additional fiber bundles, adopting nod-and-shuffle observing incurs a 50% loss in multiplex.

Is it worth it? The answer depends on whether the observing program in question is making full use of the available Fiber-WFOS multiplex. If it is, Figure 11 shows that for 1-minute sky-nodding exposures, accepting the read noise penalty in order to maintain the maximum multiplex leads to a faster overall observing speed at mid-to-redder wavelengths. Nod-and-shuffle provides an overall benefit at the bluest wavelengths, and this benefit increases on the darkest nights. An observing program targeting a sample size that is ∼70% or less than the number of available sky-object fiber bundle pairs would gain more from the improved nod-and-shuffle S/N than it would lose from the multiplex loss. This assessment is based on final noise level predictions from a long integration, but depends on the exposure time of individual frames, not on the total (summed) integration time. Note that the S/N gain from nod-and-shuffle in Figure 11 is slightly greater than expected from Equation 1 because both source and sky observations suffer a read-noise penalty. The CCD read-out time overhead has not been accounted for in this analysis. However, new CCD electronics offer ∼10 sec read-outs at 3 e^- read noise for detectors of relevant size for Fiber-WFOS. Reads of this duration could be carried out while the telescope nods and settles between alternating sky and source positions to minimize overheads.

Fiber-WFOS would enable a nod-and-shuffle mode by alternating fiber blocks along the pseudo-slit according to their location of their associated collecting bundles on the focal plane. Bundles from the inner 50% of the focal plane (i.e., at $R/R_{max} \lesssim 0.7$) would alternate with bundles from the outer half. By inserting a focal plane mask designed to block light incident on the outer 50% of the focal plane, the fibers in that region would go dark, providing un-illuminated detector storage space for the shuffling of charge recorded by the inner fiber bundles, which would be used exclusively for nod-and-shuffle observations.

B.4 Smoothing Gains at Lower Spectral Resolution

The desire to have the Fiber-WFOS spectrographs maintain fixed gratings precludes an optimized "low-resolution" mode. However, *smoothing* the standard higher-resolution spectra offers gains in S/N for programs that do not require $R \sim 5000$. The question of how close the S/N boost from smoothing matches what one would obtain in a spectrograph optimized for, e.g., $R \sim 1600$, depends on the amplitude of the read noise (σ_R) compared to the background flux.

This can be seen by examining Figure 12 and computing the S/N for the central pixel in the smoothed case (middle rows) as compared to the central pixel (and only one shown) in the low-resolution case (bottom rows). Starting with an imagined spectrograph configuration optimized for low-resolution input and setting $S_\Sigma = S_2 + S_3 + S_4$, we have:

$$\mathrm{S/N_{low}} = \frac{S_\Sigma}{\sqrt{S_\Sigma + \sigma_R^2}} \tag{2}$$

while for the central pixel of the smoothed spectrum, we find:

$$\mathrm{S/N_{smooth}} = \frac{S_\Sigma}{\sqrt{S_\Sigma + 3\sigma_R^2}} \tag{3}$$

Taking the ratio tells us how much better an optimized low-resolution mode would be compared to smoothing,

$$\frac{\mathrm{S/N_{low}}}{\mathrm{S/N_{smooth}}} = \frac{\sqrt{S_\Sigma + 3\sigma_R^2}}{\sqrt{S_\Sigma + \sigma_R^2}} = \frac{\sqrt{1 + 3\frac{\sigma_R^2}{S_\Sigma}}}{\sqrt{1 + \frac{\sigma_R^2}{S_\Sigma}}} \tag{4}$$

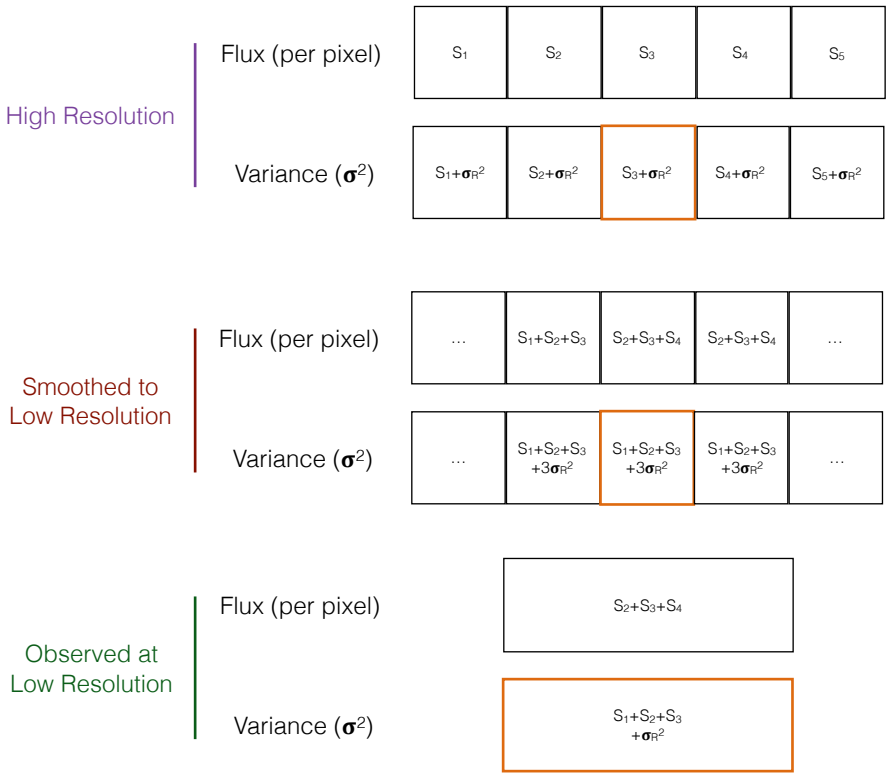

Figure 12: Flux and noise considerations for higher resolution spectra smoothed to lower resolution versus optimized low-resolution spectra. A set of 5 pixels in a medium-resolution (e.g., $R \sim 5000$) spectrum is shown schematically at the top. Each pixel has recorded a certain number of photo-electrons, S_i. The corresponding variance in each pixel (including read noise, σ_R) is shown just below. We then apply a simple 3-pixel boxcar smoothing, where each new pixel (maintaining the same size in wavelength) records the sum of its own counts with its neighbors. In the bottom set, we illustrate a single pixel with a 3 times larger wavelength size optimized to sample a 3 times lower resolution input spectrum. The comparison of the flux and variance in the central pixel in all cases allows us to measure the benefits of smoothing.

Referring to Section **??**, if we assume that 20 background counts are registered in a single CCD pixel (with 3 e^- read noise) in a 1-minute exposure, we find that an optimized instrument would provide a low-resolution S/N 1.3 times greater than smoothing (a factor of 1.6 in relative exposure time). Stated another way, the maximum S/N boost from switching from $R \sim 5000$ to $R \sim 1600$ is a factor of 1.8, but smoothing 1-minute exposures at $R \sim 5000$ still provides a S/N gain of 1.4. If 3-minute exposures were acceptable, smoothing yields a gain of 1.6, and if longer exposures were possible (e.g., with non-local sky subtraction or nod+shuffle), read noise would be negligible and the maximum boost of 1.8 is possible.

It should be noted that an additional cost of smoothing is the inefficient use of detector pixels which then oversample the resulting low-resolution spectrum. Because of correlated noise between pixels, binning or resampling of smoothed spectra does not provide further S/N gains.

References

Dawson, K., Frieman, J., Heitmann, K., et al. 2018, ArXiv e-prints, arXiv:1802.07216

Glazebrook, K., & Bland-Hawthorn, J. 2001, PASP, 113, 197

Gu, M., Conroy, C., Law, D., et al. 2017, ArXiv e-prints, arXiv:1709.07003

Halverson, S., Roy, A., Mahadevan, S., et al. 2015, ApJ, 806, 61

Law, D. R., Yan, R., Bershady, M. A., et al. 2015, AJ, 150, 19

Newman, J. A., Abate, A., Abdalla, F. B., et al. 2015, Astroparticle Physics, 63, 81

Rodrigues, M., Cirasuolo, M., Hammer, F., et al. 2012, in SPIE, Vol. 8450, Modern Technologies in Space- and Ground-based Telescopes and Instrumentation II, 84503H

Yan, R., Tremonti, C., Bershady, M. A., et al. 2016, AJ, 151, 8